Jalili et al. International Journal of Industrial Chemistry 2013, 4:33
http://www.industchem.com/content/4/1/33

International Journal of Industrial Chemistry (IJIC)
a SpringerOpen Journal

RESEARCH Open Access

DFT investigations on the interaction of oxygen reduction reaction intermediates with Au (100) and bimetallic Au/M (100) (M = Pt, Cu, and Fe) surfaces

Seifollah Jalili[1], Asghar Zeini Isfahani[2] and Razieh Habibpour[1*]

Abstract

Background: Density functional theory was used to demonstrate how the presence of second metals can modify the adsorption energies of oxygen reduction intermediates on Au (100) surfaces. Taking the importance of the modification of oxygen reduction reaction in fuel cell activity into consideration, the adsorption energy and the stable adsorption sites for the intermediates of this reaction in Au (100) and bimetallic Au/M (100) (M = Pt, Cu, and Fe) systems were closely examined. After optimization of the structures, calculations of the density of states, *d*-band center, electron charge transfer, and adsorption energies of the intermediates of oxygen reduction reaction were accomplished.

Results: The *d*-band center has been shown to be shifted because of strain and ligand effects in these bimetallic systems. The important role of hydroxyl species (OH) on catalytic surfaces was revealed while studying intermediates of oxygen reduction reaction. Hydroxyl species are strongly adsorbed on the catalytic surfaces and decrease the kinetic of oxygen reduction reaction by occupying the active adsorption sites.

Conclusions: Au-Pt-Au (100) has the biggest OH adsorption energy. Therefore, it can be concluded that the presence of the submonolayer of Pt in this bimetallic system has helped hydroxyl species occupy the active sites, and consequently, it is not an appropriate catalyst for oxygen reduction reaction.

Keywords: Bimetals, Au (100), Oxygen reduction reaction, Density functional theory

Background

One of the key goals of catalyst manufacturing is to develop new materials that have novel catalytic properties. It is possible to design catalysts with superior properties by alloying two or more metals [1,2]. Bimetallic catalysts are shown to have reactivities unlike those of the monometallic catalysts [3,4]. They are extensively used in many catalytic and electrocatalytic applications [5]. Bimetallic surfaces are produced by replacing either the submonolayer or overlayer coverage of a single crystal with an admetal. The presence of these surfaces has brought about a wide range of new chemical, electronic, and physical properties in catalysis industry. The electronic and chemical properties of a metal in a bimetallic surface may change due to two important factors. The first factor is the ligand effect that is the formation of the hetero-atom bonds. It modifies the electronic structure of the metal surface by changing its electronic environment. The second factor is the strain effect that modifies the electronic structure by changing the orbital overlap. The strain effect is manifested by the different average metal-metal bond lengths in bimetallic surfaces in comparison with those of the parent metal surfaces. However, since the strain and ligand effects usually appear together, it is complex to differentiate between them even in surface science investigations [6].

Kitchin et al. [7] have used density functional theory (DFT) calculations to demonstrate the ligand effect; they have shown that the existence of sublayer 3*d* metals in Pt (111) surfaces expands the Pt surface *d*-band. It was found that the width of the surface *d*-band is relative to the

* Correspondence: razihabibi@gmail.com
[1]Department of Chemistry, K. N. Toosi University of Technology, P. O. Box 15875–4416, Tehran, Iran
Full list of author information is available at the end of the article

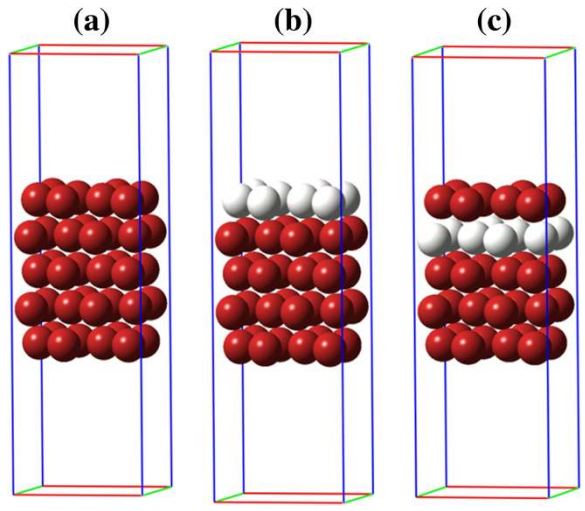

Figure 1 Side view images of monometallic Au (100) and bimetallic Au/M (100) surfaces. (a) Five-layered Au (100) slab, **(b)** five-layered bimetallic Au-M (100) slab, and **(c)** five-layered bimetallic Au-M-Au (100) slab. M = Pt, Cu, and Fe.

interactions between the *d* orbitals of the Pt surface atoms and the *d* orbitals of the subsurface 3*d* metal atoms. Because of the band broadening, the average energy of the Pt (111) *d*-band goes down in order to compensate for the *d*-band filling, and this will change the surface chemical properties.

Likewise, using the DFT calculations, the strain effect was shown to modify the chemical properties of surfaces by shifting the average energy of the *d*-band (*d*-band center) [8].

The poor oxygen reduction kinetics on Pt electrodes has stimulated the study of oxygen reduction on other bimetallic catalysts [9-12]. One of the most active catalysts for the electrochemical reduction of oxygen is Au (100) in alkaline solution, which exhibits an even higher activity than polycrystalline Pt. It is remarkable however that gold single-crystal electrodes show exceptional structural selectivity toward water or hydrogen peroxide. On Au (111) electrodes, the reduction of oxygen proceeds as a two-electron process to hydrogen peroxide, whereas on Au (100), the product will depend on the pH of the solution. In acidic media, the reduction proceeds as a two-electron process, whereas in alkaline solution, it is a four-electron process [13].

In the current study, we examine oxygen reduction on Au/M (100) (M = Pt, Cu, and Fe) using density functional theory, focusing on the effect of the presence of a second metal on the adsorption of oxygen reduction reaction intermediates on bimetallic Au/M (100) (M = Pt, Cu, and Fe) surfaces.

Methods

Computational details

Calculations were carried out within the framework of density functional theory using the Quantum Espresso v4.1, which is a DFT code based on plane wave basis sets. Electron-ion interactions are demonstrated using the projected augmented wave method, which was expanded within a plane wave basis, setting up a cutoff energy of 50Ry (≈680.2eV). Electron exchange and correlation effects were described by the generalized gradient approximation of Perdew et al. known as PW91 [14]. Brillouin zone integration was performed using a $3 \times 3 \times 1$ Monkhorst Pack grid. The Au and Au/M (M = Pt, Cu, and Fe) surface calculations were performed using face-centered cubic (fcc) (100) surfaces modeled by 2×2 unit cells of five substrate layers. A vacuum space equivalent to eight layers is utilized to detach the slab from the slabs of the upper and lower cells. In this way, there were no interactions between the adsorbed intermediates and the bottom surface of the next slab. All metal layers were allowed to relax using the Hellman-Feynman forces computed at each geometry step.

The pseudomorphic overlayer bimetallic structures (Au-M) were built by replacing the topmost layer of Au (100) slabs with a layer of the appropriate metals (Pt, Cu, and Fe). The pseudomorphic submonolayer bimetallic structures (Au-M-Au) were built by replacing the second layer of Au (100) slabs with a layer of the

Table 1 Structural and energetic parameters for pure Au (100) and bimetallic pure Au/M (100) slabs

	Optimized interlayer separation (Å) and relaxation percentage for each interlayer distance			
Surface	**First-second interlayer**	**Second-third interlayer**	**Third-fourth interlayer**	**Fourth-fifth interlayer**
Au (100)	2.96 (+2.77%)	2.98 (+3.47%)	2.98 (+3.47%)	2.96 (+2.77%)
Au-Pt (100)	2.86 (−0.69%)	2.94 (+2.08%)	2.94 (+2.08%)	2.93 (+1.73%)
Au-Cu (100)	2.64 (−8.33%)	2.98 (+3.47%)	2.95 (+2.43%)	2.93 (+1.73%)
Au-Fe (100)	2.61 (−9.37%)	2.99 (+3.82%)	2.95 (+2.43%)	2.93 (+1.73%)
Au-Pt-Au (100)	2.87 (−0.35%)	2.87 (−0.35%)	2.94 (+2.08%)	2.93 (+1.73%)
Au-Cu-Au (100)	2.69 (−6.59%)	2.72 (−5.55%)	2.98 (+3.47%)	2.93 (+1.73%)
Au-Fe-Au (100)	2.67 (−7.29%)	2.70 (−6.25%)	3.10 (+7.64%)	2.93 (+1.73%)

Positive relaxation values denote interlayer extension. Negative relaxation values denote interlayer contraction.

Table 2 Electronic properties of pure Au (100) and bimetallic pure Au/M (100) slabs

Surface	*d*-band center relative to E_f (eV)		Fractional *d*-band filling		Density of *d* states at Fermi level
	First layer	Second layer	First layer	Second layer	(states/eV)
Au (100)	−1.99	−2.49	0.9705	0.9677	0.41
Au-Pt (100)	−0.84	−2.86	0.9068	0.9637	5.51
Au-Cu (100)	−1.05	−3.02	0.9803	0.9652	0.52
Au-Fe (100)	−1.52	−3.23	0.8872	0.9649	0.72
Au-Pt-Au (100)	−2.01	−0.93	0.9671	0.8958	0.76
Au-Cu-Au (100)	−3.04	−1.87	0.9696	0.9753	0.55
Au-Fe-Au (100)	−3.21	−1.64	0.9668	0.8802	0.77

appropriate metals (Pt, Cu, and Fe). The lattice constant of the bimetallic Au/M (100) systems is determined by the experimental lattice constant of the substrate element, Au (100), that is equal to 4.080 Å. We first determined the lattice constant of face-centered cubic Au to be 4.183 Å that is in good agreement with experimental value (4.08 Å). We obtained the same surface relaxation results for the Au (100) slab with both experimental and DFT lattice constants. Moreover, we found that the Au (100) slab with both experimental and DFT lattice constants has approximately equal oxygen adsorption energies on adsorption sites. On the other hand, in a detailed

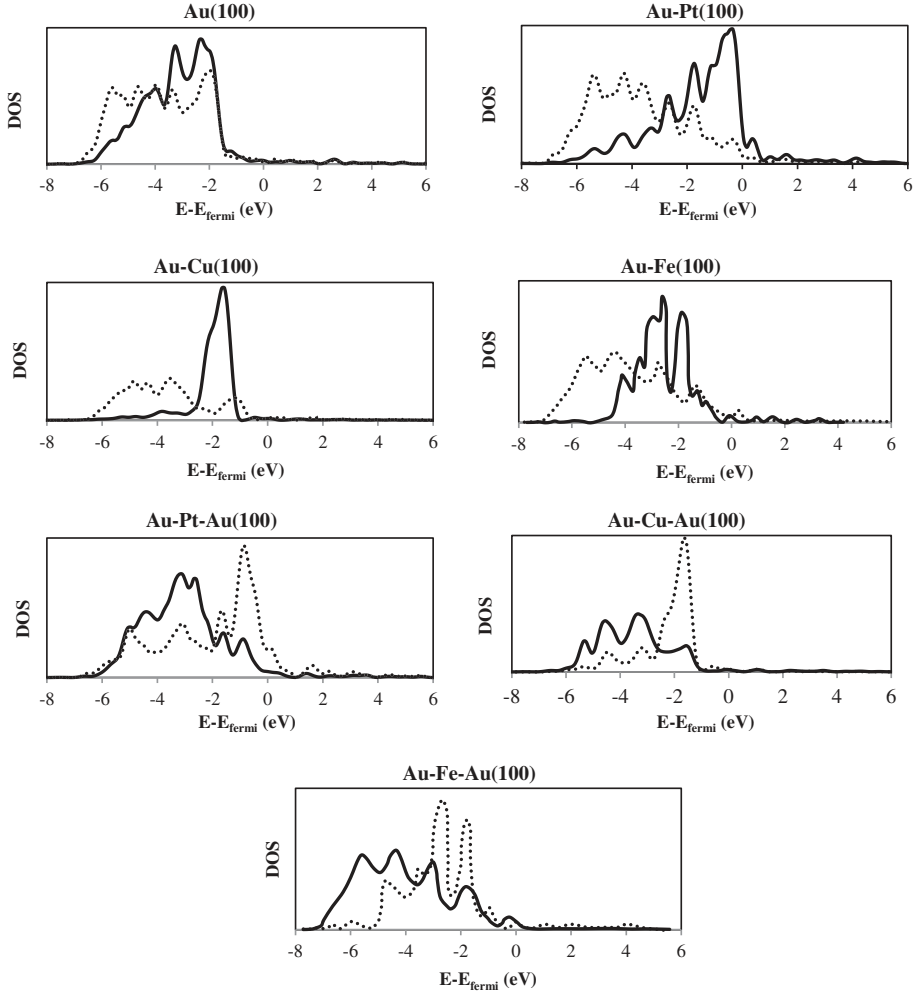

Figure 2 DOS projected to the *d*-band of the first and second metal layers for pure slabs. The first metal layer is represented by a solid line, while the second metal layer is represented by a dashed line. The Fermi level is the energy zero in all cases.

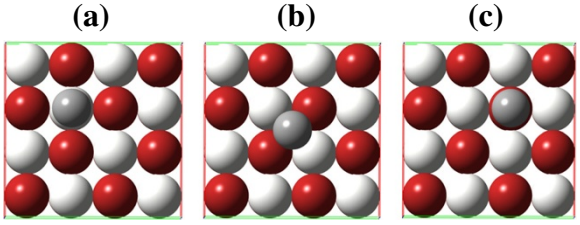

Figure 3 Top view of M (100) 2 × 2 surface. The red circles show the topmost metal atoms, and the white circles show metal atoms in the second layer. Gray circle shows the **(a)** hollow site, **(b)** bridge site, and **(c)** top site.

analysis of some of the catalytic systems, the thermodynamic stability of the bimetallic surfaces is important to consider. However, in our study, it was not taken into consideration since we are investigating the trends in oxygen reduction reaction intermediate chemisorptions on the Au/M (100) bimetallic systems. So, we decided to use the experimental lattice constant. Both the overlayer and the submonolayer bimetallic structures were relaxed to find out the optimized interatomic distance of neighboring atoms in subsequent layers.

In all systems, the adsorption energy of intermediates is calculated according to the following equation:

$$E_{\mathrm{ad}} = -\frac{1}{n}\left[E_{\mathrm{nA/slab}} - (E_{\mathrm{slab}} + nE_{\mathrm{A}})\right], \quad (1)$$

where n is the number of adsorbate intermediates in the surface of the unit cell, and $E_{\mathrm{nA/slab}}$, E_{slab}, and E_{A} represent the total energies of an intermediate adsorption system, a pure relaxed surface, and an intermediate, respectively.

Table 3 E^{O}_{ad} and $d_{O\text{-}S}$ at the coverage of 0.125 ML for each adsorption site

		Hollow	Bridge	Top
Au (100)	E^{O}_{ad} (kJ/mol)	275.07	275.60	186.41
	$d_{O\text{-}S}$ (nm)	0.104	0.141	0.189
Au-Pt (100)	E^{O}_{ad} (kJ/mol)	403.44	417.96	310.04
	$d_{O\text{-}S}$ (nm)	0.102	0.139	0.187
Au-Cu (100)	E^{O}_{ad} (kJ/mol)	427.79	403.11	280.37
	$d_{O\text{-}S}$ (nm)	0.101	0.137	0.185
Au-Fe (100)	E^{O}_{ad} (kJ/mol)	386.72	345.01	297.53
	$d_{O\text{-}S}$ (nm)	0.101	0.137	0.185
Au-Pt-Au (100)	E^{O}_{ad} (kJ/mol)	279.50	283.38	196.37
	$d_{O\text{-}S}$ (nm)	0.104	0.140	0.190
Au-Cu-Au (100)	E^{O}_{ad} (kJ/mol)	275.55	268.80	188.55
	$d_{O\text{-}S}$ (nm)	0.106	0.141	0.189
Au-Fe-Au (100)	E^{O}_{ad} (kJ/mol)	280.71	277.39	191.63
	$d_{O\text{-}S}$ (nm)	0.111	0.137	0.178

The gas-phase molecular oxygen and molecular oxygen adsorbed on the surface were simulated spin-unrestricted in order to account for the unpaired electrons on the molecule. All other systems were computed spin-restricted.

Results and discussion

Surface characterization

The monometallic Au (100) and bimetallic Au/M (100) surfaces examined in this paper are shown in Figure 1. The monometallic slab is composed of five Au layers. The bimetallic pseudomorphic overlayer surfaces are composed of five metal layers with Pt, Cu, or Fe in the first and Au in the other four underneath layers. Au-M (100) in this text stands for a pseudomorphic monolayer of M on an Au (100) surface. On the other hand, in bimetallic pseudomorphic submonolayer surfaces, Pt, Cu, or Fe atoms construct the second layer. Moreover, Au-M-Au (100) stands for pseudomorphic submonolayer of M in an Au (100) slab.

All slabs are constructed according to an fcc crystal structure with an experimental lattice constant of the substrate element, Au (100), that is equal to 4.080 Å. Therefore, at the preliminary geometry, the interlayer spaces were set to the experimental bulk value of 2.884 Å for Au (100). Then, the geometry was relaxed to obtain the optimized interlayer distance for each structure. Table 1 illustrates the optimized interlayer separation for each slab. Relaxation values that are computed in relation to the experimental bulk interlayer distance are reported in percentages. The values were calculated according to the equation below:

$$\text{Relaxation percentage} = \frac{\text{Interlayer distance (after relaxation)} - \text{Interlayer distance (before relaxation)}}{\text{Interlayer distance (before relaxation)}} \times 100, \quad (2)$$

where the interlayer distance (before relaxation) is equal to 2.884 Å. Interlayer distances (after relaxation) for all slabs are reported in Table 1.

According to these DFT calculations, the relaxation value for the Au (100) surface is not remarkable. The topmost layer of the Au (100) surface was seen to spread out with 2.77%. There is very little surface relaxation for the bimetallic Au-Pt (100) surface. Unlike the surface extension in Au (100), the top layer in Au-Pt (100) contracts to the bulk with 0.69%. Because of stronger interactions of the surface layer with the substrate layers in Au-Cu (100) and Au-Fe (100) slabs, the relaxations are larger than that of Au (100). The top layers in Au-Cu (100) and Au-Fe (100) contract to the bulk with 8.33% and 9.37%, respectively. To compensate for the enhanced electronic charge density due to contraction of

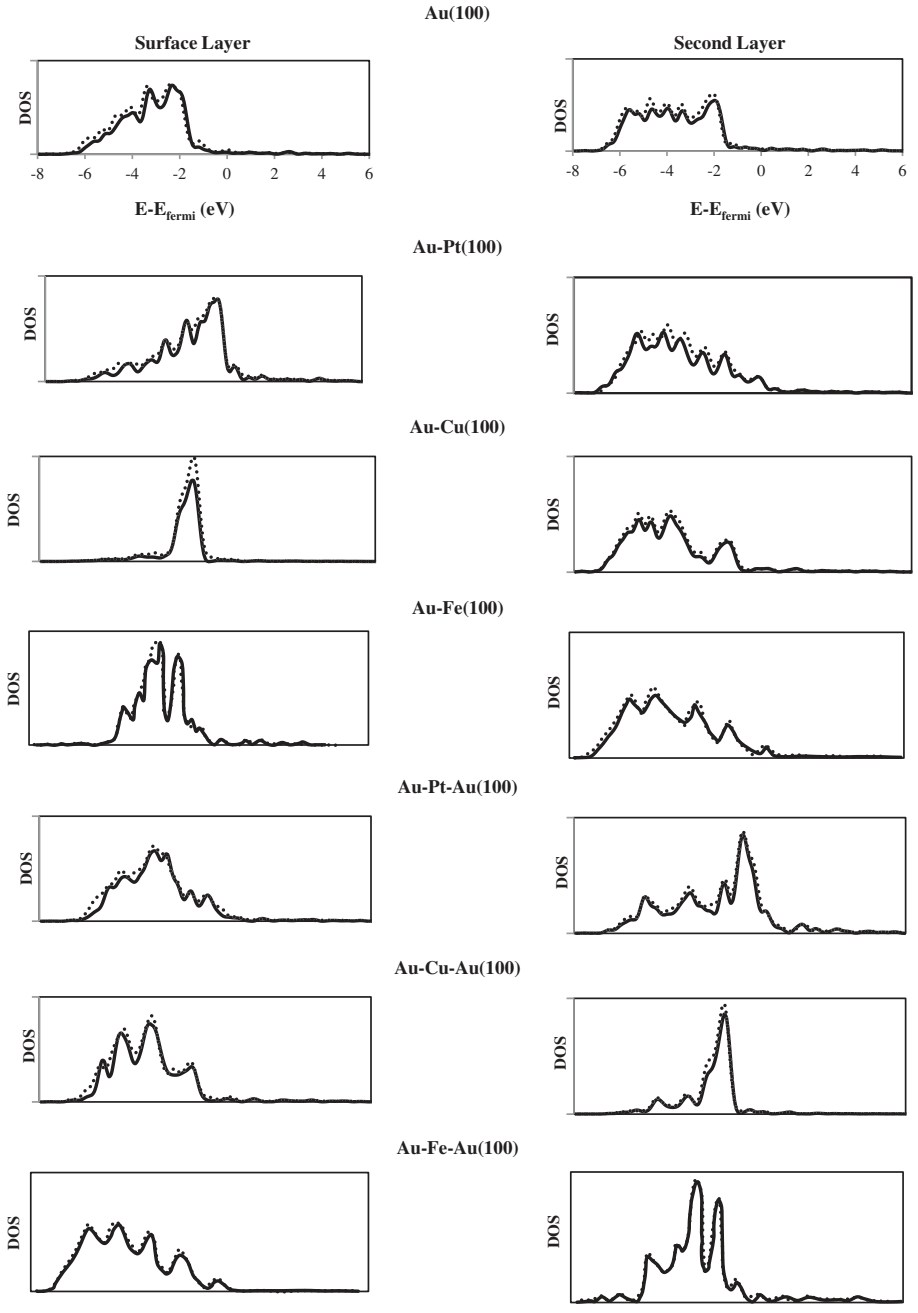

Figure 4 Effect of oxygen adsorption on projected DOS of the *d*-band in pure slabs. Solid lines represent the DOS projected to the *d*-band of pure slab. Dotted lines represent the DOS projected to the *d*-band of the oxygen-chemisorbed system, *d*-band of the topmost layer (left), and *d*-band of the second layer (right). The Fermi level is the energy zero in all cases.

the surface layers in Au-Cu (100) and Au-Fe (100), the second Au layer was seen to spread out with 3.47% and 3.82% away from the third metal layer, respectively. The maximum amount of surface relaxation is seen in Au-Fe (100) with a contraction of about 9.37%. Surface relaxation in the bimetallic Au-Pt-Au slab is very small. Unlike the surface extension in Au (100), the first and second layers in Au-Pt-Au (100) close to the bulk with 0.35%. In the bimetallic Au-Cu-Au (100), the second metal layer closes to the bulk with 5.55% similar to the first metal layer (with 6.59%). To compensate for the enhanced electronic charge density due to contraction of the first and second layers in bimetallic Au-Cu-Au, the third Au layer was seen to spread out with 3.47% away from the fourth metal layer. It was remarkably noticed that in submonolayer bimetallic systems, again, the

Table 4 Charge changes of metallic slab and atomic oxygen in Au (100) and bimetallic Au/M (100) systems

		ΔQ
Au (100)-O	Au (100) slab	−0.374
	Atomic oxygen	+0.351
Au-Pt (100)-O	Au-Pt (100) slab	−0.302
	Atomic oxygen	+0.292
Au-Cu (100)-O	Au-Cu (100) slab	−0.415
	Atomic oxygen	+0.402
Au-Fe (100)-O	Au-Fe (100) slab	−0.381
	Atomic oxygen	+0.366
Au-Pt-Au (100)-O	Au-Pt-Au (100) slab	−0.438
	Atomic oxygen	+0.409
Au-Cu-Au (100)-O	Au-Cu-Au (100) slab	−0.342
	Atomic oxygen	+0.320
Au-Fe-Au (100)-O	Au-Fe-Au (100) slab	−0.416
	Atomic oxygen	+0.397

system containing Fe, i.e., Au-Fe-Au (100), has the maximum amount of surface contraction. It is observed that Au-Fe-Au (100) has the most amount of expansion in the third and fourth layers. The metal layers of the substrate in the bimetallic Au-M (100) slabs display relaxations similar to those the monometallic Au (100) systems. For example, the second metal layer (i.e., the first Au layer in substrate layers) of the Au-Pt (100) slab spreads out with 2.08% which is approximately equivalent to the relaxation of the surface layer of the Au (100) slab (+2.77%). Likewise, the second metal layer of the Au-Cu (100) surface spreads out with 3.47%, which is comparable with the expansion of the surface layer of the Au (100) surface (+2.77%). In all bimetallic Au-M-Au (100) surfaces except Au-Fe-Au (100), the third to fourth metal layers display relaxations similar to those of the second to third metal layers in the corresponding bimetallic Au-M (100) slabs. The results indicate a smaller Au/M interlayer distance for Au-M (100) surfaces in comparison to the topmost Au/M interlayer distance in corresponding Au-M-Au (100) surfaces. This fact implies stronger Au/M interaction in Au-M (100) surfaces.

Table 5 Structural and energetic information of molecular oxygen adsorption

System	$R_{M1\text{-}O1}$ (Å)	$R_{M2\text{-}O2}$ (Å)	$R_{O\text{-}O}$ (Å)	E_{ad} (kJ/mol)	Stable adsorption site
Au (100)	2.27	2.29	1.34	510.86	Bridge
Au-Pt-Au (100)	2.28	2.29	1.43	531.12	Hollow
Au-Cu-Au (100)	2.37	2.38	1.31	502.13	Bridge
Au-Fe-Au (100)	2.28	2.27	1.45	542.51	Hollow

The electronic properties for pure Au (100) and pure bimetallic Au/M (100) slabs are illustrated in Table 2. The location of the *d*-band center relative to the Fermi level was utilized to analyze the chemisorption of adsorbates on metal surfaces [15,16]. This parameter determines the amount of interaction between the adsorbate orbital states and metal *d* states for electron donation and backdonation [17]. The *d*-band center is defined as the first-order moment of the normalized projected density of states (DOS) about the Fermi level. The various moments of the DOS for one specific orbital or total sum of orbitals are determined using the following equation:

$$\mu_n = \frac{\int_{-\infty}^{+\infty} \varepsilon^n \rho(\varepsilon - \varepsilon_0)\, d\varepsilon}{\int_{-\infty}^{+\infty} \rho(\varepsilon - \varepsilon_0)\, d\varepsilon}, \quad (3)$$

where n is the order of the moment, ρ is the density of states, ε is the energy, and ε_0 is the reference energy which is usually set to the Fermi energy. The total normalized number of states is defined by the zeroth-order moment ($n = 0$) of DOS. The average energy of the DOS, i.e., DOS 'band center', is determined by the first-order moment ($n = 1$) [18]. The fractional filling of the *d*-band was also obtained by integrating the area under the projected DOS up to the Fermi level. The DOS projected to the *d*-band of the first and second metal layers in each of the pure slabs are shown in Figure 2. The broadening of the *d*-band for the surface metal atoms in bimetallic Au-M-Au (100) slabs is because of the strong electronic interaction of the Au overlayer with the M (Pt, Cu, and Fe) layer. The broadening of the *d*-band and the unchanged *d*-band filling in the toplayer cause the surface *d*-band center in Au-Pt-Au (100), Au-Cu-Au (100), and Au-Fe-Au (100) surfaces to move down 0.02, 1.05, and 1.22eV, respectively, in comparison with Au(100). A comparison of the *d*-band center of the second layer in Au (100) with that of Au-Pt (100), Au-Cu (100), and Au-Fe (100) indicates that the surface metal atoms have had a large effect on the *d*-band. These findings indicate that by using different bimetallic combinations, the value of the surface *d*-band center that is directly related to surface chemical properties can be easily controlled. The effects of such modification will be illustrated all over the remainder of this paper. For more detailed information, please refer to our previous work [19].

Oxygen reduction reaction intermediates and their interactions with Au (100) and bimetallic Au/M (100) (M = Pt, Cu, and Fe) surfaces

In the following sections, we discuss the individual intermediates on the Au (100) and bimetallic Au/M (100) surfaces.

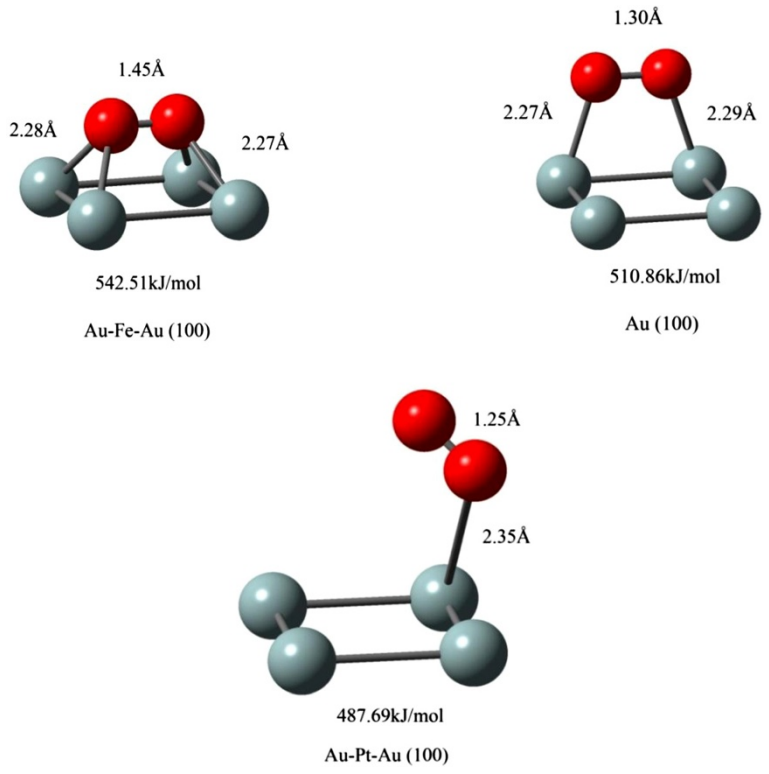

Figure 5 Hollow, bridge, and top configurations, energies of adsorption, and geometry specifications of an oxygen molecule on surfaces.

Molecular and atomic oxygen

Various adsorption sites were considered including top, bridge, and hollow sites with different orientations of the adsorbates (flat, end-on, and tilted). For each of the adsorption sites, only the results for the most stable orientation are presented.

A detailed study on atomic oxygen adsorption taking the effect of surface oxygen coverage into consideration is provided in our previous work [19].

In the first place, in order to study the adsorption of one oxygen atom on the Au (100) 2 × 2 and Au/M (100) 2 × 2 surfaces, E_{ad}^{O} was obtained. It actually means the coverage, Θ, of 0.125 ML for each surface. As shown in Figure 3, we examined three adsorption sites (hollow, bridge, and top) for all surfaces.

For each adsorption site, E_{ad}^{O} and $d_{O\text{-}S}$ (the distance between O and the surface) are listed in Table 3. It was found that in the Au (100) surface, even though $d_{O\text{-}S}$ in the bridge site is longer than that in the hollow site, the bridge site is 0.53 kJ/mol more stable than the hollow site. It is an unremarkable difference; we can conclude that those two sites are evenly populated at low coverages.

The values of E_{ad}^{O} for the hollow and bridge sites are larger than the values for the top site in all surfaces. This is because of the low coordination of the top site that is not favorable for adatom binding on transition metal surfaces. In bimetallic Au-M-Au (100) slabs, there is very little change in E_{ad}^{O} when compared to monometallic Au (100). This little difference in adsorption energy, considering the precision of the DFT technique, causes the assumption that both Au (100) and bimetallic Au-M-Au (100) slabs have similar strengths of adsorption for oxygen. However, for the bimetallic Au-M (100) slabs, oxygen adsorption energy is very high. The maximum value of E_{ad}^{O} (427.79 kJ/mol) is related to the Au-Cu (100) surface which is in good agreement with the large contraction in this surface (–8.33%).

Table 6 Structural and energetic information of hydroperoxyl adsorption

System	$R_{M1\text{-}O1}$ (Å)	$R_{M2\text{-}O2}$ (Å)	$R_{O\text{-}O}$ (Å)	E_{ad} (kJ/mol)	Stable adsorption site
Au (100)	2.13	-	1.44	204.78	Top
Au-Pt-Au (100)	2.26	3.11	1.47	325.93	Hollow
Au-Cu-Au (100)	2.33	3.52	1.46	386.62	Hollow
Au-Fe-Au (100)	2.29	3.23	1.47	311.24	Hollow

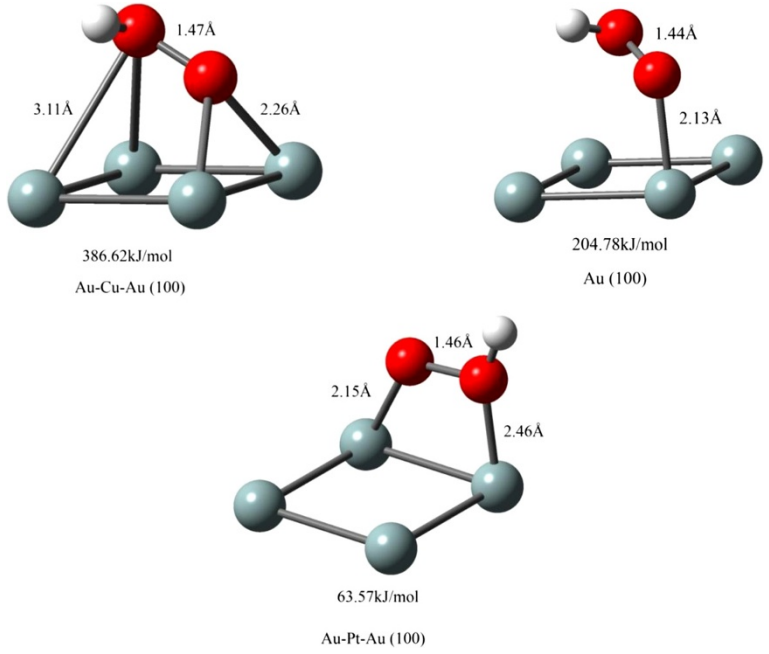

Figure 6 Hollow, bridge, and top configurations, energies of adsorption, and geometry specifications of HO_2 species on surfaces.

The *d*-band density of states for the surface and second metal layer in both the pure and oxygen-chemisorbed systems are shown in Figure 4. There is a small disturbance in the electronic DOS for the second metal layers. However, the *d*-bands for the surface layers of Au (100) and Au/M (100) systems are changed by oxygen adsorption. This change is considerable in Au-Cu (100) and Au-Pt (100).

The differences in the oxygen atom adsorption on the Au (100) and Au/M (100) surfaces are also investigated by the adsorption-induced changes in the Löwdin charges. We obtained the Löwdin charge (the number of valence electrons) of each atom in the supercell system from the Löwdin population analysis based on the projected electron densities of states. The total Löwdin charges for Au (100) and Au/M (100) slabs were obtained by making a sum of the Löwdin charges of all atoms in them. Table 4 gives the charge changes (ΔQ) for slabs and atomic oxygen in different supercell systems, which were calculated by subtracting the Löwdin charge of the corresponding component in its isolated form from that in the optimized adsorption structures. A positive value of ΔQ will imply a gain of electrons by the component. When an oxygen atom is adsorbed on the metallic surfaces, the oxygen atom is negatively charged. It can be seen that the largest loss of a Löwdin charge of *ca.* 0.438 *e* by the metallic slab and the largest charge gain of about the same amount (0.409 *e*) by the atomic oxygen occur upon the oxygen adsorption on the Au-Pt-Au (100) system. Therefore, it can be concluded that the presence of the second metal plays a fundamental role in the modification of the electronic properties of bimetallic surfaces. Further analysis indicates that the charge loss of the Au (100) and M/Au (100) slabs occurs mainly in their *d* orbitals, and the gained charges in atomic oxygen mainly go to *p* orbitals. This means that a *d-p* charge transfer between the metallic substrate and atomic oxygen occurs in the chemisorption process. It should be pointed out that the values of ΔQ given in Table 4 may not represent the exact charge gain/loss for each component in the supercell systems since some parts of the 'delocalized' or 'bonding' charges may be missed in such calculations. These charges may be located in regions that are not included in the atomic orbitals within which the LDOS are integrated to obtain Löwdin charges. In DFT calculations, the atomic orbitals used for charge calculations

Table 7 Structural and energetic information of hydroxyl adsorption

System	R_{M1-O} (Å)	R_{M2-O} (Å)	E_{ad} (kJ/mol)	Stable adsorption site
Au (100)	2.21	2.23	173.38	Bridge
Au-Pt-Au (100)	2.18	2.20	201.87	Bridge
Au-Cu-Au (100)	2.21	2.24	174.13	Bridge
Au-Fe-Au (100)	2.21	2.22	182.25	Bridge

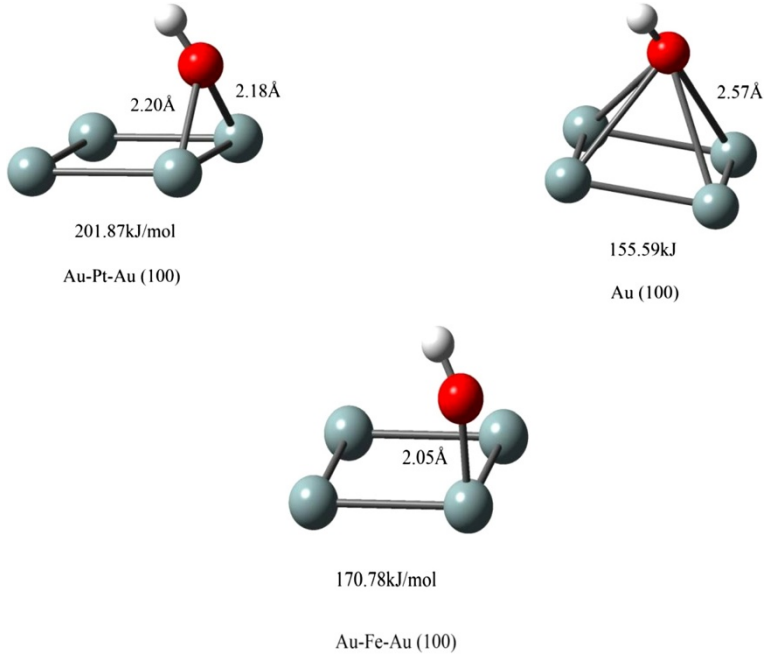

Figure 7 Hollow, bridge, and top configurations, energies of adsorption, and geometry specifications of OH species on surfaces.

are arbitrary to some extent [20]. In addition, some charges may also spill out into the vacuum region in some cases [21]. Due to the same reasons, the Löwdin charges (as well as other conventional atomic charges) do not satisfy a sum rule. For example, the Löwdin charge gain of atomic oxygen does not exactly match the value of charge loss by the metallic slab in magnitude. However, this would not refute the fact that charge transfer does occur.

Molecular oxygen on the Au (100) or Au/M (100) surfaces could be formed upon adsorption of O_2 molecules from the solution or from the gas phase [13].

$$O_2 + Au \rightarrow O_2/Au \quad (4)$$

Structural and energetic parameters of O_2 adsorption are shown in Table 5. All of the three adsorption sites - hollow, bridge, and top - are stable in O_2 adsorption. The most stable appears to be the hollow site in Au-Fe-Au (100) with the molecule lying flat on the surface. For the bridge site, the most stable configuration is the molecule lying flat on the surface in Au (100). On the top adsorption site, in Au-Pt-Au (100), the molecule is in the tilted configuration. This state is characterized by a longer Au-O distance from the surface of 2.35 Å, suggesting a rather weak chemical interaction compared to the hollow or bridge sites (Figure 5).

In molecular oxygen adsorption as well as atomic oxygen adsorption, the oxygen molecule is charged due to electron charge transfer from the metal surface. The electron charge transfer occurs from the conduction band of the metal to the $2\pi^*$ molecular orbitals of O_2. The change of the electronic state is also clearly reflected in the O-O bond distance, which increases in the same order of states from 1.25 Å in Au-Pt-Au (100), which is comparable to the gas-phase isolated O_2 molecule, to 1.45 Å in Au-Fe-Au (100). On the top site, the oxygen molecule retains its original charge state (Figure 5). Different 'charged' states of the molecular oxygen are observed as a result of the very close proximity (on eigenvalue energy scale) of the $2\pi^*$ molecular orbitals (MOs) of molecular oxygen to the Fermi level (i.e., the highest occupied electron band of the metal). On different adsorption sites, and thus by different local chemical and electrostatic environments, the $2\pi^*$ MOs are above or (partially) below the Fermi level, resulting in a (partial) electron transfer.

Table 8 Structural and energetic information of H_2O_2 dissociation into two adsorbed OH radicals

System	R_{M1-O1} (Å)	R_{M2-O2} (Å)	E_{ad} (kJ/mol)	Stable adsorption site
Au (100)	2.01	2.30	169.85	Top
Au-Pt-Au (100)	1.97	2.28	200.11	Top
Au-Cu-Au (100)	2.02	2.29	170.21	Top
Au-Fe-Au (100)	2.04	2.32	178.89	Top

Hydroperoxyl (HO_2)

In the oxygen reduction reaction, hydroperoxyl HO_2 intermediates on the metal surface could be formed in a couple of ways:

$$O_2/\mathrm{Au} + H_2O + \mathrm{Au} \rightarrow HO_2/\mathrm{Au} + \mathrm{HO/Au} \quad (5)$$

This is a purely chemical reaction, i.e., there isnot any charge transfer through the interface.

The second way is

$$O_2/\mathrm{Au} + H^+_{(aq)} + e^- \rightarrow HO_2/\mathrm{Au} \quad (6)$$

This is an electrochemical step involving a hydronium ion H^+ (aq) from the solution and an electron e^- from the cathode. The overall formation reaction of HO_2/Au from O_2 and H_2 is

$$O_2 + \frac{1}{2}H_2 + \mathrm{Au} \rightarrow HO_2/\mathrm{Au}. \quad (7)$$

In all the calculated cases, HO_2 is stable, and no dissociated form is found. To calculate the binding energies, the HO_2 radical is taken as a reference in the gas phase, with a O-O bonding distance of 1.35 Å, O-H distance of 0.99 Å, and O-O-H angle of 104.96°. After adsorption, the molecule tilts on top of two metal atoms; this is due to the weaker interaction of the OH side of the molecule with the surface. In all cases, as it can be expected, the bonding is realized primarily through the non-H-bonded oxygen atom of the HO_2. For the bridge and hollow configurations, one could guess that an additional bond is being formed through the second oxygen atom. In all cases, the HO_2 species are charged as a result of an electron charge transfer from the metal surface. The adsorption energies and geometries are listed in Table 6, and Figure 6 shows the geometries over the surfaces.

Hydroxyl (OH)

Hydroxyl on the surface could be formed via

$$\mathrm{O/Au} + H_2O + \mathrm{Au} \rightarrow 2\mathrm{HO/Au} \quad (8)$$

$$HO_2/\mathrm{Au} + H_2O \rightarrow H_2O_2 + \mathrm{HO/Au} \quad (9)$$

$$H_2O_2 + 2\mathrm{Au} \rightarrow 2\mathrm{HO/Au} \quad (10)$$

$$\mathrm{O/Au} + H^+_{(aq)} + e^- \rightarrow \mathrm{HO/Au}. \quad (11)$$

The overall formation reaction of HO/Au is

$$\frac{1}{2}O_2 + \frac{1}{2}H_2 + \mathrm{Au} \rightarrow \mathrm{HO/Au}. \quad (12)$$

Hydroxyl is maybe one of the most important oxygen reduction reaction intermediates; experimental data imply that it adsorbs strongly on the catalyst surface blocking active sites [22] and that its degree of interaction with different transition metal surfaces is an important indication of its efficiency toward oxygen reduction. In all surfaces in this study, the preferred adsorption site for hydroxyl is found to be the bridge site. At a higher OH concentration, a hydrogen bond is formed between adsorbed neighbor OH species. This effect further stabilizes the OH groups. The OH species can be considered as negatively charged due to electron charge transfer from the metal surface. The adsorption energies and geometries are listed in Table 7, and Figure 7 shows the geometries over the surfaces.

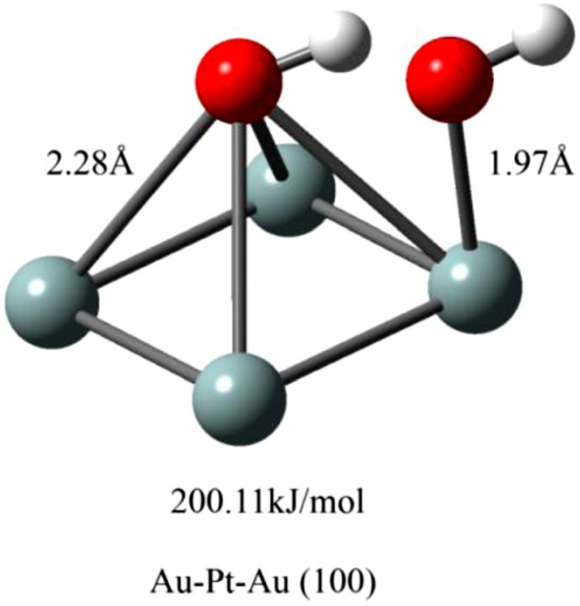

Figure 8 Configuration of adsorption, energy of adsorption, and geometry specifications of H_2O_2 species on Au-Pt-Au (100).

Hydrogen peroxide (H_2O_2)

Formation of H_2O_2 could occur as a result of a chemical reaction between OOH and water (9) or after electrochemical reduction of OOH:

$$HO_2/\mathrm{Au} + H^+_{(aq)} + e^- \rightarrow H_2O_2 + \mathrm{Au} \quad (13)$$

The overall formation reaction of H_2O_2 is

$$H_2 + O_2 \rightarrow H_2O_2. \quad (14)$$

The most stable electronic configuration for H_2O_2 is a singlet with bond lengths of 1.47 Å for O-O and 0.98 Å for O-H, angles of about 100° for H-O-O, and a dihedral angle of about 112°. We were not able to find stable adsorption sites of H_2O_2 on the studied surfaces. When it is placed over a surface, dissociation is observed in all systems. After dissociation, two OH species are observed only in one configuration, where one OH adsorbs on the top site and the other is in a near-hollow position for all studied surfaces. The adsorption energies and geometries are

listed in Table 8, and Figure 8 shows the geometries over the surfaces.

The density of states for adsorption on Au (100) is shown in Figure 9. All adsorbates are similar in that they exhibit a bonding peak with the O-*p* electrons overlapping the bottom of the Au *d* band. Molecular oxygen as well as the hydroperoxyl exhibits a second *p*-electron peak below the bonding peak, which is characteristic of the π bond between the two oxygen atoms. The hydropyroxyl exhibits an additional peak composed of *s* and *p* electron densities resulting from the O-H bond. This *sp* peak is also apparent in OH, where only one *p*-electron peak exists. Only atomic oxygen does not feature a second peak immediately below its *p*-electron overlap with the *d* band. Therefore, adsorption of these intermediates involves two phenomena: bonding and antibonding interactions in agreement with the Hammer and Norskov model for adsorption [23]. Peaks of *p*-orbital states related to O-O bonds are also present above the *d* band for O_2 and HO_2 adsorption.

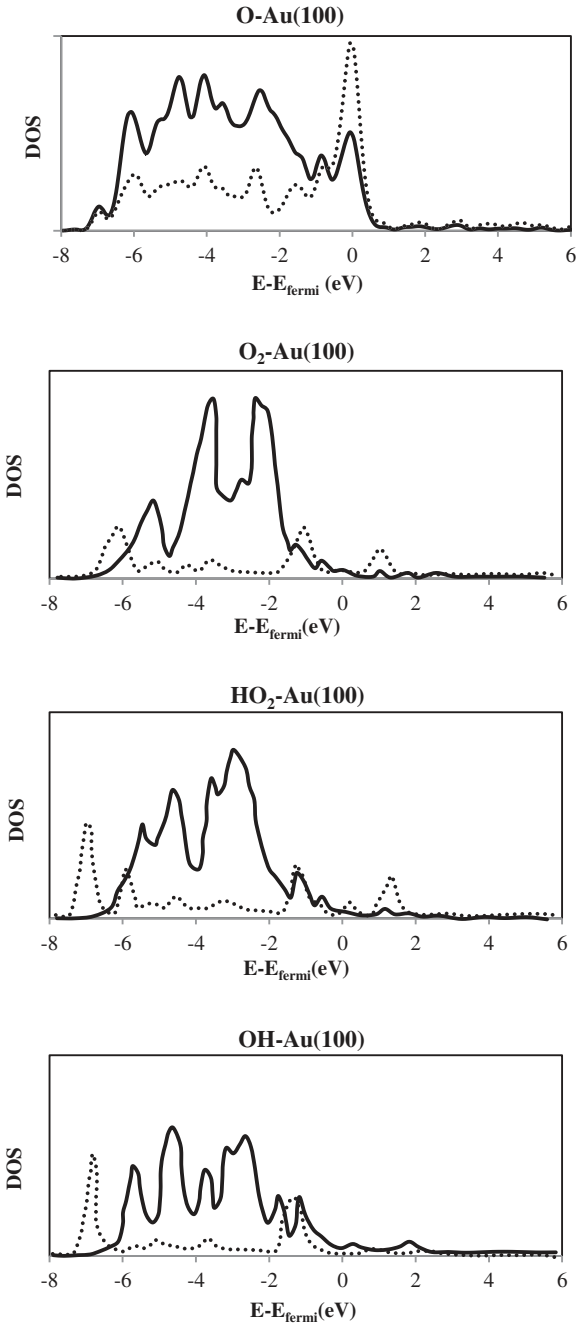

Figure 9 Projected DOS for adsorption of intermediates on monometallic Au (100). The Fermi level is the energy zero in all cases. Solid lines represent the DOS projected to the *d*-band of Au (100). Dotted lines represent the DOS projected to the *d*-band of the intermediates.

Experimental

The background of all our work is the solution of Schrödinger's equation to describe the interactions of atoms in a solid modeled by two- or three dimensionally periodic arrangements of atoms. In principal, no empirical parameters are needed for our calculations. The only - and crucial - approximation has to be made for the many-body interaction of the electrons surrounding the atomic nuclei which is done in the framework of density functional theory. Because of the fundamental approach, our calculations require substantial computational costs depending on the size of the systems, i.e., the number of atoms in the unit cell. Systems of 50 to 100 atoms can still be reasonably treated on the fastest machines including workstations. Therefore, we constantly work on optimization of codes and methods and on providing sufficient access to the most powerful computer systems available. On the other hand, a first-principles approach allows the treatment of all types of atoms and many different systems with the same machinery. Therefore, the spectrum of systems which are studied is huge, ranging from free atoms, clusters, bulk solids, interfaces, surfaces, and molecules on surfaces. For such systems, important physical and chemical properties can be derived solely based on hard numbers without any empirical parameters.

Conclusions

DFT calculations were performed on Au (100) and bimetallic Au/M (100) (M = Pt, Cu, and Fe) surfaces to understand how the presence of the second metal can influence the adsorption of intermediates of the oxygen reduction reaction. The adsorption energy of hydroxyl is probably an important factor in the determination of the surface's resistance to inhibition of the oxygen reduction reaction, while the O and O_2 adsorption energies help to determine the kinetically limited steps.

By weakening the hydroxyl adsorption, the catalyst surface become more resistant to hydroxyl accumulation, and therefore, it eliminates the repulsion interaction of oxygen reduction intermediates. Au-Pt-Au (100) has the biggest

hydroxyl adsorption energy. Therefore, it can be concluded that the presence of the submonolayer of Pt in this bimetallic system has helped hydroxyl species occupy the active sites, and consequently, it is not an appropriate catalyst for oxygen reduction reaction.

Competing interests
The authors declare that they have no competing interests.

Authors' contributions
SJ participated in the interpretation of results. AZI read and edited the manuscript and commented on it. RH conducted all the experiments mentioned in the manuscript, analyzed the data, and drafted the manuscript. All authors read and approved the final manuscript.

Acknowledgments
The authors wish to gratefully acknowledge the facilities provided by the University of Isfahan.

Author details
[1]Department of Chemistry, K. N. Toosi University of Technology, P. O. Box 15875–4416, Tehran, Iran. [2]Department of Chemistry, University of Isfahan, P. O. Box 81746–73441, Isfahan, Iran.

Received: 9 December 2012 Accepted: 16 February 2013
Published: 22 May 2013

References
1. Calvo SR, Balbuena PB (2007) Density functional theory analysis of reactivity of Pt_xPd_y alloy clusters. Surf Sci 601:165–171
2. Mei DH, Hansen EW, Neurock M (2003) Ethylene hydrogenation over bimetallic Pd/Au (111) surfaces: application of quantum chemical results and dynamic Monte Carlo simulation. J Phys Chem B 107:798–810
3. Roudgar A, Gross A (2005) Water bilayer on the Pd/Au (111) overlayer system: coadsorption and electric field effects. Chem Phys Lett 409:157–162
4. Sadek MM, Wang LC (2006) Effect of adsorption site, size, and composition of Pt/Au bimetallic clusters on the CO frequency: a density functional theory study. J Phys Chem A 110:14036–14042
5. Carabineiro SAC, Thompson DT (2010) Gold catalysis. In: Corti C, Holliday R (ed) Gold: science and applications. Taylor & Francis Group, New York
6. Chen JG, Menning CA, Zellner MB (2008) Monolayer bimetallic surfaces: experimental and theoretical studies of trends in the electronic and chemical properties. Surf Sci Rep 63:201–254
7. Kitchin JR, Nørskov JK, Chen JG, Barteau MA (2004) Modification of the surface electronic and chemical properties of Pt (111) by subsurface 3*d* transition metals. J Chem Phys 120:10240–10246
8. Mavrikakis M, Hammer B, Nørskov JK (1998) Effect of strain on the reactivity of metal surfaces. Phys Rev Lett 81:2819–2822
9. Dae-Suk K, Tae-Jun K, Jun-Hyuk K, Abo-Zeid EF, Yung-Tae K (2010) Fine structure effect of PdCo electrocatalyst for oxygen reduction reaction activity: based on X-ray absorption spectroscopy studies with synchrotron beam. J Electrochem Sci Thec 1:31–38
10. Wang C, Li D, Chi M, Pearson J, Rankin RB, Greeley J, Duan Z, Wang G, Vliet D, More KL, Markovic NM, Stamenkovic VR (2012) Rational development of ternary alloy electrocatalysts. J Phys Chem Lett 3:1668–1673
11. Paulus UA, Wokaun A, Scherer GG, Schmidt TJ, Stamenkovic V, Radmilovic V, Markovic NM, Ross PN (2002) Oxygen reduction on carbon-supported Pt – Ni and Pt – Co alloy catalysts. J Phys Chem B 106:4181–4191
12. Stamenkovic V, Schmidt TJ, Ross PN, Markovic NM (2002) Surface composition effects in electrocatalysis: kinetics of oxygen reduction on well-defined Pt_3Ni and Pt_3Co alloy surfaces. J Phys Chem B 106:11970–11979
13. Yeager E (1986) Dioxygen electrocatalysis: mechanism in relation to catalyst structure. J Mol Catal 38:5–25
14. Perdew JP, Chevary JA, Vosko SH, Jackson KA, Perdsen MR, Singh DJ, Fiolhais C (1992) Atoms, molecules, solids, and surfaces: applications of the generalized gradient approximation for exchange and correlation. Phys Rev B 46:6671–6687
15. Hammer B, Nørskov JK (1995) Electronic factors determining the reactivity of metal surfaces. Surf Sci 343:211–220
16. Hammer B, Morikawa Y, Norskov JK (1996) CO chemisorption at metal surfaces and overlayers. Phys Rev Lett 76:2141–2144
17. Pallassana V, Neurock M, Hansen LB, Hammer B, Norskov JK (1999) Theoretical analysis of hydrogen chemisorption on Pd(111), Re(0001) and Pd_{ML}/Re(0001), Re_{ML}/Pd(111) pseudomorphic overlayers. Phys Rev B 60:6146–6154
18. Kitchin JR, Nørskov JK, Barteau MA, Chen JG (2004) Role of strain and ligand effects in the modification of the electronic and chemical properties of bimetallic surfaces. Phys Rev Lett 93:156801–156804
19. Jalili S, Zeini Isfahani A, Habibpour R (2012) Atomic oxygen adsorption on Au (100) and bimetallic Au/M (M = Pt and Cu) surfaces. Comp Theor Chem 989:18–26
20. Valencia F, Romero AH, Ancilotto F, Silvestrelli PLJ (2006) Lithium adsorption on graphite from density functional theory calculations. Phys Chem B 110:14832–14841
21. Nduwimana A, Gong XG, Wang XQ (2003) Relative stability of missing-row reconstructed (110) surfaces of noble metals. Appl Surf Sci 219:129–135
22. Stamenkovic V, Schmidt TJ, Ross PN, Markovic NM (2003) Surface segregation effects in electrocatalysis: kinetics of oxygen reduction on polycrystalline Pt_3Ni alloy surfaces. J Electroanal Chem 554:191–199
23. Hammer B, Norskov JK (2000) Theoretical surface science and catalysis - calculations and concepts. In: Gates BC, Knozinger H (ed) Impact of surface science on catalysis. Academic, San Diego, CA

doi:10.1186/2228-5547-4-33
Cite this article as: Jalili *et al.*: **DFT investigations on the interaction of oxygen reduction reaction intermediates with Au (100) and bimetallic Au/M (100) (M = Pt, Cu, and Fe) surfaces.** *International Journal of Industrial Chemistry* 2013 **4**:33.